On demand nanoliter-scale microfluidic droplet generation, injection, and mixing using a passive microfluidic device

Uwe Tangen, Abhishek Sharma, Patrick Wagler, and John S. McCaskill[a)]
Faculty of Chemistry and Biochemistry, Microsystems Chemistry and BioIT (BioMIP), Ruhr-University Bochum, 44780 Bochum, Germany

(Received 19 December 2014; accepted 29 January 2015; published online 12 February 2015)

We here present and characterize a programmable nanoliter scale droplet-on-demand device that can be used separately or readily integrated into low cost single layer rapid prototyping microfluidic systems for a wide range of user applications. The passive microfluidic device allows external (off-the-shelf) electronically controlled pinch valves to program the delivery of nanoliter scale aqueous droplets from up to 9 different inputs to a central outlet channel. The inputs can be either continuous aqueous fluid streams or microliter scale aqueous plugs embedded in a carrier fluid, in which case the number of effective input solutions that can be employed in an experiment is no longer strongly constrained (100 s–1000 s). Both nanoliter droplet sequencing output and nanoliter-scale droplet mixing are reported with this device. Optimization of the geometry and pressure relationships in the device was achieved in several hardware iterations with the support of open source microfluidic simulation software and equivalent circuit models. The requisite modular control of pressure relationships within the device is accomplished using hydrodynamic barriers and matched resistance channels with three different channel heights, custom parallel reversible microfluidic I/O connections, low dead-volume pinch valves, and a simply adjustable array of external screw valves. Programmable sequences of droplet mixes or chains of droplets can be achieved with the device at low Hz frequencies, limited by device elasticity, and could be further enhanced by valve integration. The chip has already found use in the characterization of droplet bunching during export and the synthesis of a DNA library.

[http://dx.doi.org/10.1063/1.4907895]

I. INTRODUCTION

As biochemical processing volumes decrease to the picoliter volumes typical of cells, and beyond, general purpose fluid handling, especially pipetting and mixing processes, needs to miniaturize from the microliter scale.[1,2] In special configurations, smaller volumes already allow thousands to millions of samples for combinatorial experimentation,[3] down to the single molecule scale,[4] saving costly time and material. Although major achievements have been made in nanoliter to picoliter processing,[5,6] general purpose pipetting solutions are still predominantly integrated with liquid handling robots at the multi-microliter scale,[2] and the more integrated technologies such as "digital microfluidics," using EWOD (electrowetting on dielectric),[7,8] currently still operate at near μl droplet scales (0.3 μl). Earlier work using integrated electroosmotic pumps without droplets[9] did not provide sufficient general purpose functionality and reliability to yield a nanoliter scale equivalent for liquid handling robots. This paper investigates a further step towards general programmability of droplet processing at the nanoliter

a)Author to whom correspondence should be addressed. Electronic mail: john.mccaskill@rub.de.

scale, which has already been applied to DNA library production.[10] DNA library synthesis is a typical combinatorial application where a direct addressable interface to integrated downstream processing is needed, although a technique for maintaining addressable identity of droplets during export has been developed using our combinatorial droplet generator.[11]

Although very large numbers of mechanical microvalves (tens of thousands) have been integrated onto microfluidic chips, for example, using the multiplex pressure addressing system employed by Quake,[12] allowing direct nanoliter processing, the cost and effort to produce and operate these solutions have directed these developments to special biotechnological problems, where a particular process or protocol is required, rather than yielding generally programmable processing devices. For example, the Fluidigm assay chip Dynamic Array IFC performs a particular pairwise mixing between two sets of up to 96 samples at the scale of nanoliters, but cannot perform higher order mixtures or other processes. Droplet processors have successfully bridged the gap down to nanoliter and picoliter scales, by avoiding mechanical boundaries in favor of phase boundaries, but the achievement of general purpose droplet processing equivalent to pipetting robots at the nanoliter scale has proved difficult, despite significant progress. This paper aims to contribute to this issue by focusing on a general purpose programmable pipetting at the nanoliter scale inside microfluidic devices, and taking one step further in the programmable complexity of such devices.

Droplet technologies have been extensively reviewed[6,8,13] along with their surfactants.[14] The most mature droplet dispensing technology involves inkjet printing, with, for example, piezo-driven expulsion and capillary action refilling of a defined volume, and works efficiently down to picoliter volumes when a limited number of larger volume fluids with carefully matched viscosities are employed. The recent HP/Tecan picoliter digital dispensing product,[15] working with a single solution at a time, currently restricts the choice of solvent (to DMSO (dimethylsulfoxide) in current commercial products). The general use of multiple print heads to dispense mixtures is limited by the effort required to uptake multiple solutions programmably and to process without loss the resulting nanoliter scale droplets. The creation of droplets within a microchannel facilitates downstream droplet processing, but complicates both the expulsion mechanism and the reservoir filling process. Apart from the combinatorial advantage, droplet segmentation also permits the transport of heterogeneous solutions,[16] such as time varying samples or samples with concentration gradients.

Significant efforts have been made to establish droplet-on-demand (DoD) technology that supports programmable multi-channel mixing of solutions at the nanoliter scale or below.[17] It is comparably straightforward to generate regular streams of droplets, either through passive T-, Y-, K-, or higher order junctions or through an active oscillatory process[18] as in pressure-, piezo-, or electrostatically driven droplet chains. Single DoD, require the control impulse to activate a clean single cycle and return to a resting non-generating state ready for the next trigger impulse. Pressure driven control of DoD up to now requires a stiff valve system integrated near the point of action[19] or on-chip valves.[20] In these cases, valves are created in adding a second layer in the microstructure, usually PDMS (polydimethylsiloxane) with device scales of ca. 500 μm. These valves are driven by externally applied air-pressure, with each nozzle requiring at least one fluidic and one air channel. To select the valves, usually more air-pressure channels are required per nozzle.[21] In addition to these static DoD systems, dynamic creation of DoDs[22] uses the surface tension between the sample and the carrier-fluid, typically water in oil, to pinch off a droplet with a sudden-pressure impulse on the built-in valve, but the reported sensitivity of the interface makes it unlikely that this principle may be used for more than one or two nozzles in the same microfluidic flow system.

Active in-chip, nanoliter scale, DoD generation and injection, with programmability expandable in the number of input solutions, allows for possible on-chip integrated processing prior to export from the chip. This is in contrast with direct droplet dispensing techniques (e.g., HP/Tecan above). On chip DoD generation utilizes an array of mechanisms (i) integrated mechanical microvalves,[23] micropumps[24] or piezo-based pressure modulators,[25,26] (ii) external pressure control from off-chip valves,[19] (iii) electrokinetic impulses to control droplet formation,[27] (iv) electrowetting based control of droplet formation,[7,8] (v) electrochemical gas

formation or laser-induced cavitation[28] to drive droplet expulsion, (vi) electrorheological control of ferrofluid spacers to control droplet formation,[29] (vii) ultrasound for nanoliter droplet ejection,[26] and (viii) electro-hydrodynamic droplet printing[30] especially in-chip.[31] Of special note is the kHz frequency picoinjector technique[27] that requires electronic integration on chip with 30 V drivers for each channel, operating via electrical droplet interface destabilization, and achieving rms injection variations of about 25% at 1 pl volumes.

This paper will employ commercially available off-chip pumps and valves in conjunction with a novel passive microfluidic chip to support parallel combinatorial generation and mixing of nanoliter droplets in-chip. As we shall explain, the parallel (8 to 10) independently controlled in-chip nozzles do not limit the number of different solutions that can be mixed. Sequentially indexed plug flow allows one to interface our microfluidic chip to array formats such as microwell plates (MWPs), as also proposed for extending the input flexibility of DoD systems.[32]

The structure of the paper is as follows. Section II covers the diverse experimental materials and methods necessary to design, fabricate, operate, and evaluate the nanoliter processing system for DNA libraries. Section III presents our results on in-chip nanoliter droplet generation and injection and compares our system with simulation results, starting with physical characterization of droplets. The main results are: (i) the optimized combinatorial DoD microfluidic chip; (ii) robust valve-controlled programmable droplet generation and injection; (iii) a semi-automated plug injection system for combinatorial input from MWPs; and (iv) the microscope-assisted droplet export system to MWPs. Section III also evaluates our achievements in the light of previous work, and finally in Section IV we summarize the consequences for general programmable nanoliter scale fluid handling and future directions. Extensive supplementary material is available.[35]

II. MATERIALS AND METHODS

A. Microfabrication

For the custom droplet-on-demand system, we adopted the dynamic DoD approach in combination with external valves (see also Sec. II B). Integrating valves increases the complexity (and cost) of devices and involves two-layer- (crossing channel) PDMS-technology that is not readily compatible with thin-layer microfluidics,[33,34] which has been optimized for high NA optical imaging (optically flat surface and short optical path length through glass and PDMS to sample), stiff pressure control and low gas permeation. Our design approach requires channel structures with two or three different depths, as explained below, but no membranes or channel crossings.

A three level microfluidic channel network was produced by soft-lithography using a silicon wafer with a multi-plane patterned photoresist combination of SU8–25/50 (Microlithography Chemical Corp., Newton, MA) that serves as a mold master. Three successive lithographic steps are employed in the fabrication flow shown in Figure 1. Fabrication starts with lithography steps (A) and (B) of the first microfluidic level, which contains the shallow 2 μm deep nozzle structures. In addition, an adhesion layer for the deep (115 μm) outlet channel was prepared. The following lithographic steps (C) and (D) lead to structuring of the I/O channels for droplet formation and transport. The final lithography (E) and (F) creates the downstream meander and output channel. For polymer molds, a mixture of PDMS prepolymer (Sylgard 184, Dow Corning) and the curing agent is cast against the fabricated master using a 125 μm thin cover glass slide (G). This cover slide improves the optical properties and increases the stiffness of the PDMS-layer and makes it possible to use mineral oil as a carrier fluid. Curing the polymer and releasing it from the master yield a replicate containing three levels of different heights for the required microchannels (H).

A series of fluidic design improvements were made to arrive at the final design shown in Figure 2. The design features a U-shaped central channel for the carrier fluid (starting at input 11) into which ten flow-by droplet nozzles enter. One nozzle for label/spacer droplets is located at the end of the carrier channel (see below). This geometry was chosen to allow compact microscopic imaging. Each nozzle is a shallow ledge structure (2 μm cf. Figure 1) separating the flow-by region from the central carrier channel. In order to ensure proper external valve control,

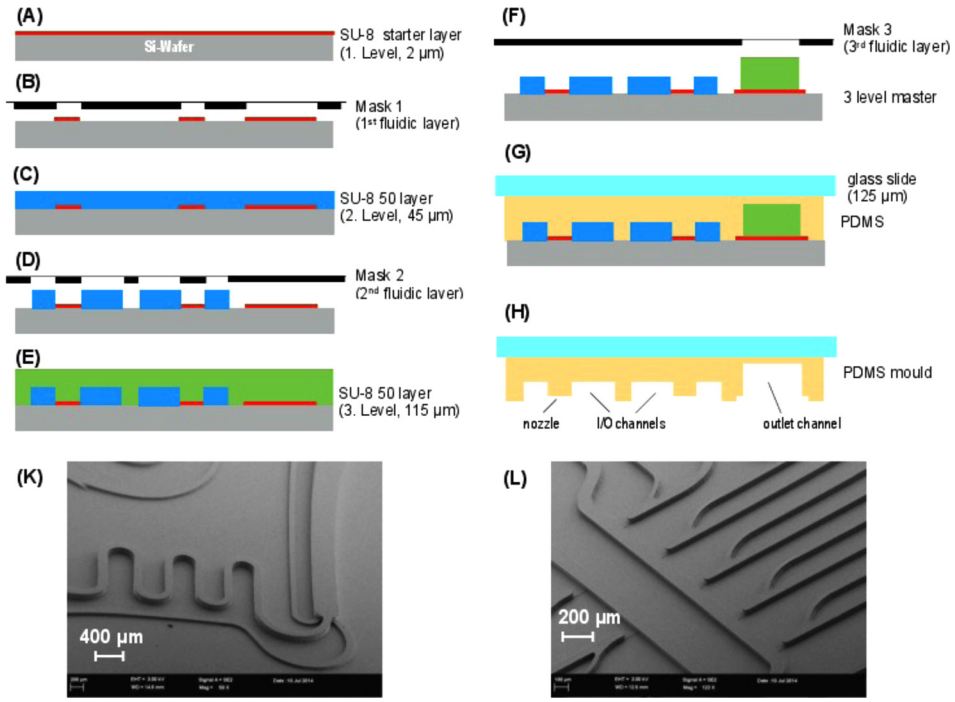

FIG. 1. Fabrication flow of three-layer lithography and PDMS micro-molding. (A) SU8-25 photoresist deposition, thickness 2 μm, (B) 1st lithography step, (C) SU8-50 photoresist deposition, thickness 45 μm, (D) 2nd lithography step, (E) SU8-50 photoresist deposition, thickness 115 μm (F) 3rd lithography step, (G) PDMS molding, (H) releasing the PDMS replica, and (K) and (L) SEM images of patterned photoresist combination of SU8-25/50.

each nozzle input (e.g., channel 8 for nozzle 1) is hydrodynamic resistance equalized via length and each output (e.g., channel 9) is resistance minimized using a larger channel width. After passing the first nine nozzles, the droplet carrier channel is routed via a series of mixing curves (at top left) back to the main residual space on the chip (lower third) where droplets can be further stabilized or re-spaced with another carrier surfactant mix (input 1).

A major problem in establishing stable droplet formation is a high hydrodynamic pressure inside the carrier fluid channel. To solve this problem, while retaining low volume input channels, we added the deeper output channel system (red, main output 25). Aqueous DNA-solution inlets (2, 4, 6, 8, 12, 14, 16, 18, 20, and 22) and outlets (3, 5, 7, 9, 13, 15, 17, 19, 21, and 23) in the microfluidic structure are used for the up to 9 injection samples. Apart from inlet 22, all aqueous inlets are pressure-equalized. The carrier fluids are usually applied to inlets 10 and 11.

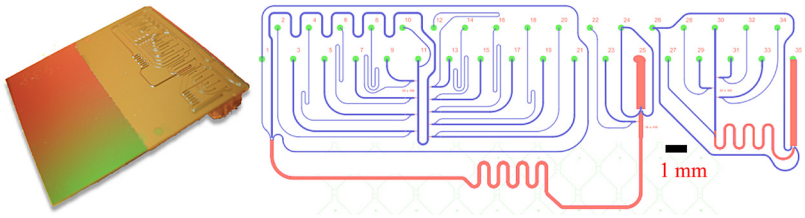

FIG. 2. Microfluidic chip for parallel nl droplet generation and injection mixing. Left: Fully assembled droplet processor on silicon with micro-molded three-layer PDMS fluidics and backside interconnection. Right: Dynamic DoD final microfluidic chip design. Inlets 2, 4, 6, 8, 14, 16, 18, 20, and 22 are used for reactants or markers and inlets 1, 10, 11, and 24 for carrier fluids, allowing for adding different surfactants or changing droplet spacing. Outlet 25 transports the created droplets into an output FEP (fluorinated ethylene propylene)-tube. All other inlets are used as backpressure ports for the droplet creation. Dimensions of nozzles (first microfluidic layer): length 80 or 100 μm, width 30 μm, and height 2 μm; second layer (height 45 μm, blue color) for I/O channels; third layer (height 115 μm, red color) for short downstream meander and output channel. The separate structure on the far right is an additional test-structure.

Inlet 10 can also be used to add surfactants to improve droplet creation. The final inlet, 24, provides additional control of droplet spacing and/or surfactant stabilization for export.

B. Fluidic control and switching architecture

Early experiments with externally driven pressure changes did not provide robust repeatable creation of single droplets. This was achieved by controlling the external pressure downstream rather than upstream to the aqueous injection microchannels, as shown in Figure 3. We used economical electric pinch valves as the programmable component for droplet formation, to allow parallel control. This change in the location of the pressure-generating device allowed abrupt reductions of pressure and reliable droplet injection without the need for samples to pass through the pressure pulsing device (reduction of possible contamination). In contrast to systems with integrated valves, our microfluidics employ hydrodynamic barriers (1–2 μm high and up to 100 μm long shallow channels), which effectively decouple the flows between the carrier fluid and the water phase. This decoupling, which is supported by the elastic properties of the PDMS, is the major reason why we are able to create nozzle-designs that work with more than two nozzles.

The geometric design of the microfluidic chip was derived from a T-junction as shown in Figure 3 and features a shallow ledge opening into a deep channel in 3D. A constant flow syringe pump (MDSP3f, Micromechatronic Technologies GmbH, Germany) was connected to the central channel with mineral oil as the carrier fluid phase—swelling of PDMS is not an issue here because of the thin packaging of the multilayer construction. The sample input side channel was connected to another constant flow pump (Syringe pump 540060, TSE Systems GmbH) with aqueous dispersed phase.

The proper droplet-on-demand nozzle control is vital to achieve reliable operation. Each sample input solution requires an outlet on the same side of the injection nozzle for flow-by operation. The output of each side channel was connected to an off-chip pinch valve (BioChem Ltd., 100P2NO12-01SM from MS-Scientific Chromatography) and then to a tunable resistor (custom design RUB), which was tuned to control the back-pressure for droplet formation, such that the two phase interface stays stable at the nozzle entrance. In the custom flow-resistors, low pitch screws are used to individually compress a silicon adapter, so that the active pressure is adjusted at each nozzle. Smaller screw pitches could make this variable flow-resistor more sensitive. A short pressure impulse is applied against the flow in the side channel using the

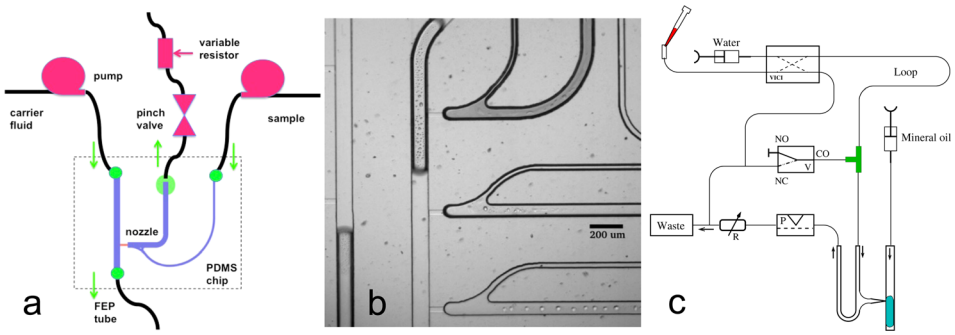

FIG. 3. Droplet-on-demand implementation scheme and combinatorial input. (a) An aqueous droplet is injected into the carrier stream, a hydrophobic fluid, with a short strong pressure pulse, created via a pinch-valve. A variable flow resistor adjusts a suitable working pressure. The essential innovation was to put the pinch-valve after the nozzle. Earlier attempts with the pressure-generating device upstream of the nozzle failed because mostly several droplets were created after the pulse. As a function of carrier fluid pressure, droplets can be injected stably only between 0.5 and 1.5 bar. (b) A close up of the real injection nozzle under white light microscopy. (c) MWP to microfluidic chip combinatorial interface. One channel out of eight is shown. From the MWP, samples are taken and injected into the VICI-valve (left upper part), and then pushed through the long plug-storing tube, separated by mineral oil. The plug train is then transported to the T-junction when VICI-valve and solenoid are activated. After filling the loop, the VICI valve is switched back into the default position and after returning the solenoid into default position the plugs are serially fed into the microfluidic structure. This flow scheme exhibited the best plug separation properties.

pinch valve, enough to cause dispersed fluid flow to the main channel through the nozzle. This leads to the formation of a droplet that could be easily programmed by manipulating the pressure impulses and respective timings. The overall experimental setup is summarized schematically in Fig. S9 of the supplementary material.[35]

A combinatorial sample plug input system can be placed in front of each of the nozzle inputs. The hardware setup for plug import and a sketch of the sample loop loading and loop operation are shown in Figure 3(c). Loading of the tube from the VICI-valves (8 ports, C2H-1348EH and 10 ports, C2H-1340EH, Valco Instr. Co. Inc. each controlling two inputs, which are located below the xy-table at the filling station) towards the T-junction is done via switching the VICI valves appropriately and opening the three-port solenoid-valves. The FEP-tubes normally employed for connections exert a too high flow resistance so that normal pipetting operations (e.g., with a Gilson pipette) were no longer possible with them. With a PTFE (polytetrafluoroethylene)-tube (inner diameter 0.8 mm), this problem could be solved, but still a low dispensing speed is a necessity. After inserting the first plug, a spacer-fluid, currently mineral oil, is added and then the next material from one of the wells of the MWP is injected. It was found that mineral oil is able to relieve air-bubbles sitting in adapters and T-junctions. Because of this, we usually add a further mineral oil plug early in the injection process to remove all remaining air in the injection system. Finally, an additional mineral oil-plug seals the whole train of plugs. When the plugs reach the T-junction the three-port solenoid is closed and the plug is fed into the microfluidic structure.

Lastly, for complete biochemical applications, we require a method of exporting droplets back to MWPs. After testing several more automated methods using solenoid and piezoelectric spotting, which were not able to preserve the multiphase fluid structure, the method of export finally used was to drop a larger (several μl big) mixed-phase droplet containing carrier fluid and a chain of combinatorial aqueous droplets directly into the well of a MWP. With a hand-held USB (universal serial bus) microscope, we can observe the falling of the drop. An active high-flow ejection stream of mineral oil, inserted by an additional low dead-volume, transparent T-junction right at the output of the system, can serve as a controlled expelling of the output-droplet. Using colored separation droplets, we could separate one droplet chain from another chain of droplets with a different mixture. This labeling of the output droplets allows the export of the mixtures without destroying droplets and minimizing the risk of contamination. In other work, we have now demonstrated how the size of these leading droplets can be reduced from μLs down to droplets almost the same size as the samples (just a few nanoliters).[11] Oil carrier separation is performed on multiple collected droplets in MWPs by plate centrifugation and subsequent pipetting of the water-phase out of the well from beneath the oil. The mineral-oil is a standard capping ingredient in microwell plates and compatible with many processes.

C. Separation fluids and surfactants

In most cases, mineral oil (Sigma Aldrich M5904-500ML, lot# MKBL2644V) and 0.02% or 0.2% Abil (EM90 from Franken-Kosmetik Chemie) was used as a carrier with surfactant. Apart from easily forming droplets (a surfactant concentration of 0.01% up to 0.2% proved to be optimal) mineral oil is a good solvent, removing debris from aggregates and impurities. Normally, mineral oil cannot be used in PDMS structures, because it dissolves and creates a swelling of the PDMS. Due to our tight sandwich structure, silicon-PDMS-glass cover,[34] the effect of swelling can be neglected, as confirmed by measuring images taken before and after 1 day of oil filling (see supplementary material[35] Fig. S14). We tested other low viscosity oils, like petroleum or gasoline, to reduce the inner pressure in the system. These tests were not successful, but despite the shorter alkane chains present in these oils, PDMS was not destroyed—the swelling being entirely reversible.

Low viscosity ionic liquid carriers were also employed (IL-0035-HP, 89.3mPas and IL-0023-HP, IoLiTec Ionic Liquids Technologies GmbH, Germany) when droplets were well spaced, but suffered from the absence of optimal surfactants for droplet stabilization. Surfactants developed to stabilize micelles in ionic liquids[45] could not be used to stabilize

larger droplets. Furthermore, ionic liquid tends to coat channel surfaces, which, after some time, become adhesive for aqueous droplets. A frequent reuse of the microfluidic structure is thus prevented. In future work, there should be sufficient flexibility in the choice of ionic liquids to achieve this.

D. Optical monitoring system for microfluidic chip and export

Laser scanning fluorescence microscopy with three color detection (488 nm, 561 nm, 640 nm excitation with linearly polarized cw excitation from DPSS (diode-pumped solid-state) and diode lasers Coherent) and AOTF (acousto-optical tunable filter) wavelength selection (BRI-MVA200, Brimrose) was employed. A line-scan fluorescence microscope (based on an Olympus IX81 inverse microscope with custom cylindrical exciter optics and an X-Y galvo-scanner, Thorlabs) was employed using primarily 4×, 10× magnification objectives. Natural food colors, bromophenol blue (4,4′-(1,1-dioxido-3H-2,1-benzoxathiole-3,3-diyl)bis(2,6-dibromophenol)) and white light illumination were also used in addition to fluorescence. For export, in addition, a portable USB-microscope (DigiMicro Profi, dnt GmbH, 27× and 100×) was employed to image droplets at the tip of a capillary during export.

E. Overall system integration

The overall system consisted of pumps, multiport- and pinch valves, resistors, two x-y tables (one for microfluidic chip and one for MWPs), three microscopes (inverse for microfluidic chip viewing, tandem for MWP viewing, and USB for export droplet viewing), multicolor laser illumination system, capillary connections, a motorized pipette mounted with z-axis, and solenoid push button control, all mounted on a passively vibration damped laser table (see supplementary material[35] Figure S9).

F. System control software

The hardware is accessed with a custom-developed software (http://fp7-matchit.eu/index.php?page=software-repository (the software is specific to the experimental hardware platform employed)), which either accesses the parallel port of the controlling PC (personal computer) or several USB-serial interfaces and consists of a number of programs and scripts. The control of the multiport- and pinch-valves is done with a short Perl-TK script.

In principle, all experiments reported in this paper could have been done with conventional microscope management software as well, like μManager (https://www.micro-manager.org/), since they do not involve microelectrode feedback control. Our custom software platform integrates all peripheries as well as supporting the integration done with the electronic layer of the microfluidic chips. This will prove beneficial in combination with separation processes, but, for those interested in applying only the results of this paper, the necessary control could be achieved by adapting standard extended microscope software.

G. Two phase flow simulation and hydrodynamic equivalent circuits

Multiphase computational fluid dynamics (CFD) simulations were performed using OpenFoam[36] in order to optimize microfluidic designs varying applied pressure, flow rates, and nozzle geometry. We used the surface-capturing Volume of Fluid (VOF) method[37] to solve the two phase fluid flow equations, tracking the interfaces between two phases using an indicator phase function γ with intermediate values only near phase boundaries

$$\gamma = \begin{cases} 1 & \text{phase 1} \\ 0 < \gamma < 1 & \text{interface} \\ 0 & \text{phase 2.} \end{cases} \quad (1)$$

Using this indicator function, momentum equations for multiple phases can be written as a single equation

$$\frac{\partial \rho \boldsymbol{U}}{\partial t} + \nabla \cdot (\rho \boldsymbol{U}\boldsymbol{U}) = -\nabla p + \nabla \cdot \boldsymbol{\tau} + \rho \boldsymbol{f} + \int_{S(t)} \sigma \kappa' \boldsymbol{n}' \delta(x - x') dS. \tag{2}$$

The first term on the left side describes the acceleration of the velocity field (U), and the second term is the convective acceleration. On the right side, the first term is the pressure gradient, τ is the stress tensor

$$\tau = \mu(\nabla U + \nabla U^T), \tag{3}$$

where f describes the acceleration due to the body forces, and the last term describes the source due to surface tension σ. Integration was carried out using the interFoam solver.[36] The Salome Platform[38] was used to design the microfluidic structures and stationary mesh generation. ParaView was used for post-processing and data visualization. Fluid flow could be assumed to be laminar at the low Reynolds numbers found in slow flows at microfluidic scales.

To complement the detailed two-phase flow models, we also employed hydrodynamic equivalent circuit modeling to optimize and characterize the device (see Sec. III E). Hydrodynamic circuit models with flow resistors, calculated using standard low Reynolds number formulae for various channel cross-sections, are now common[39] and have been used successfully in modeling complex microfluidic circuits.[40] Voltage and current translate to pressures and volume flow rates. In this work, it is necessary to make hydrodynamic circuits more realistic by including the elasticity of components using capacitors in parallel to ground (i.e., atmospheric pressure) for these resistors: with hydrodynamic capacitance or compliance being volume displacement per unit pressure. We used the QUCS circuit simulation program (http://qucs.sourceforge.net) to integrate the circuit models with a stiff solver option (Adams). Note that there are three potential sources of capacitive corrections to the stiff system (instantaneous current response resistive scheme without capacitors): the first is due to the elasticity of the channels and tube walls, the second is due to the finite relaxation time of the fluid velocity change upon change in pressure and is ignored for the small flow rates used, and the third is due to compressibility/expansion of the fluid and can safely be ignored as long as temperature variations are small.

III. RESULTS AND DISCUSSION

A. Mechanism of droplet formation by pressure impulse using nozzles

Pressure impulses applied against the flow (i.e., pinch-valve is downstream, see also Sec. II B) leads to an increase in the fluid flow in the stagnant region, (Figure 4(a)), which, when the pressure is sufficient, results in flow through the nozzle (for dynamics see supplementary material[35] Movie S1). The mechanism of droplet formation depends strongly on the duration of pressure impulses and the flow rates of dispersed and continuum phases. As soon as, the pressure impulse ends, the two-phase interface moves back, which leads to detachment of the droplet from the nozzle. Figure 4(b) shows a series of snapshots describing the droplet formation for short impulse times. The behavior of droplet formation changes when the impulse time becomes long enough, such that pressure drop at the nozzle becomes ineffective and cannot sustain fluid injection to the main channel. In this case, the detachment of droplets from the nozzle is governed by the flow rates of fluid in the two channels. This effect constrains the size of the droplet that can be formed in the microfluidic device. Figure 4(c) shows snapshots describing the droplet formation for larger impulse times, and Fig. 4(d) visualizes in parallel many droplets in a meander on a chip (using a similar droplet generator chip design). The videos in supplementary material[35] S2 and S3 document the dynamics for short

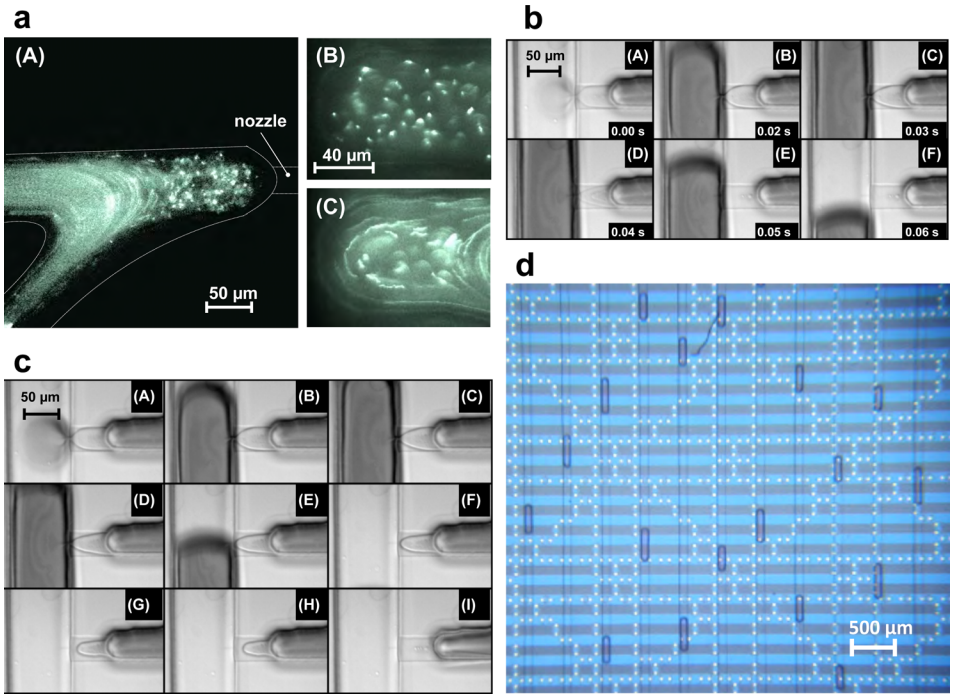

FIG. 4. Droplet formation microscope images. (a) Fluid flows in nozzles. (A) Fluid flow profile near the vicinity of the nozzle, flow rate in side channel: 100 μl/h using 100 nm size fluorescent beads, (10× magnification). (B) Magnified view region near to the nozzle tip, with stable interface (60× magnification). (C) Flow profile near the nozzle tip during droplet formation (60× magnification). (b) Stages of droplet formation with short impulse time. Flow rates in side channel: 100 μl/h, central channel: 20 μl/h, impulse time: 0.05 s. Images show (A)–(C) filling up during the pressure impulse, (D) and (E) pinch off at the end of impulse, and (F) droplet motion and interface relaxation. (c) Stages of droplet formation with long impulse time. Flow rates in side channel: 100 μl/h, central channel: 20 μl/h, impulse time: 4 s. Images show (A) and (B) filling up during the pressure impulse, (C) and (D) necking due to fall of pressure with time, (E)–(H) droplet pinch off and presence of two phase interface in the nozzle, and (I) interface retraction at the end of pressure impulse, with long relaxation time. (d) Generated droplet population on the chip. In this case, ionic liquid is used as a carrier fluid, and the aqueous droplets are observed on chip in a long meander. The microelectrodes visible below the meander structure were not used in this experiment, but confirm that our one-layer PDMS DoD system is readily integrated with other microsystem components—in this case on the substrate.

and long impulse times. As opposed to electrically switched generators,[27] our design is robust towards carrier fluids with different electrical characteristics such as the conducting ionic liquid used in Fig. 4(d).

B. Statistics of droplet generation: Single nozzle and nine nozzles

Long-term stability tests of droplet creation were conducted: in Fig. 5(a) for a single nozzle, in Fig. 5(b) for nine nozzles on the same chip, and in Fig. 5(c) for eight tuned nozzles on the chip. The nozzles were first coarsely adjusted (via the tuneable resistors) to deliver equal nanoliter volumes (to within 30%), and optionally the nozzles were finely adjusted to deliver 1 nl volumes to within 5%. In Fig. 5(b), 5 nozzles were finely adjusted via impulse time, allowing 4 individual nozzle outputs to be compared with the 5 fine-tuned volume-aligned operation. In Fig. 5(c), 8 nozzles were finely adjusted. The nozzles were operated such that no droplets collide with each other and all 9 or 8 pinch-valves were switched on in a cyclical fashion. The droplets were extracted from video microscope images and their volume measured using a custom-designed image processing software. The data from 700 droplets were analyzed as a histogram and fitted to a sum of 9 or 8 Gaussian distributions with identical amplitude and variation, confirming the low and constant (23 pl) variation in droplet volumes for single nozzles in the multi-nozzle context for both 1 nl and 2 nl scales (2.3% or 1.1%, respectively). The overall delivery performance for multiple nozzles is contingent on the

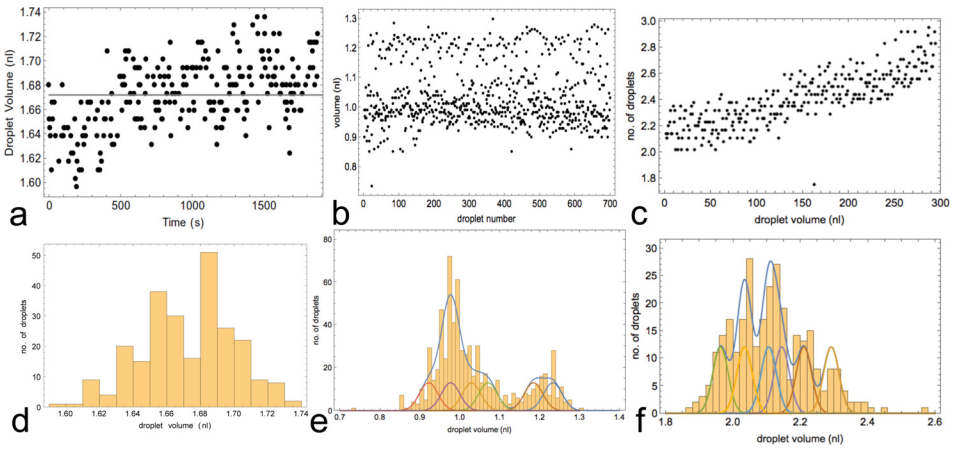

FIG. 5. Droplet-size statistics from single and nine nozzles. (a) Droplet data (252 droplets) from single operation of one of the 9 nozzles. (b) Droplets (700 droplets) generated from cycled nine working nozzles: 5 are tuned. (c) Droplets (700 droplets) generated from eight tuned cycled nozzles. (d) Histogram of droplets from single nozzle (see (a)). (e) Histogram of droplets from nine nozzles (see (b)). (f) Histogram of droplets from 8 tuned nozzles (see (c)). Image processing to extract droplets and measure sizes was done via custom software. The droplet-size was set to about 1 nl (a) and (b) and 2 nl (c). In b(e), 5 nozzles were volume matched to 1 ± 0.05 nl, and 4 others were only tuned to within 30%, so that their droplets could be discriminated by volume. In c(f), all 8 nozzles were tuned to 2.1 ± 0.1 nl. Also shown in (e) and (f) is a fit to a sum of equal amplitude and variance Gaussians corresponding to the 9 or 8 nozzles, respectively. In (e), the common fitted rms deviation was 23 pl (i.e., 2.3%), and in (c) 23 pl (i.e., 1.1%). In (e), the fit produces 4 identical Gaussians with mean volume 0.98 nl and 1 with 1.03 nl, i.e., 5 inside 5%, the other 4 fitted nozzle means are 0.92, 1.07, 1.18, and 1.23 nl corresponding to the four 30%-adjusted nozzles (see text). In (f), the fit of the 8 tuned and drift-corrected nozzles produces 8 Gaussians with means 1.96, 2.03, 2.03, 2.11, 2.11, 2.14, 2.21, and 2.29 nl.

tuning process. The more nozzles that are active in the flow-system, the longer it takes to get the whole system stably tuned: compare the time stable Fig. 5(b) with uniform drift in Fig. 5(c). Examples of calibration curves for fine tuning nozzles are shown in supplementary material[35] Fig. S10.

C. Droplet on demand size regulation

The droplet size created by the nozzle is increased with the duration of pressure impulses created by the pinch valves, see Figure 6, saturating at a finite impulse time of about 0.2 s. However, after each pressure impulse, the two-phase interface takes a finite time to relax and retrieve its original position so that the magnitude of the response also depends on the time gap between pulses. The relaxation time of the two-phase interface depends primarily on the flow rate in the flow-by side channel. The faster the flow rate of fluid in the side channel, the smaller is the relaxation time (compare Figs. 6(a) and 6(b)). These effects occur due to strong

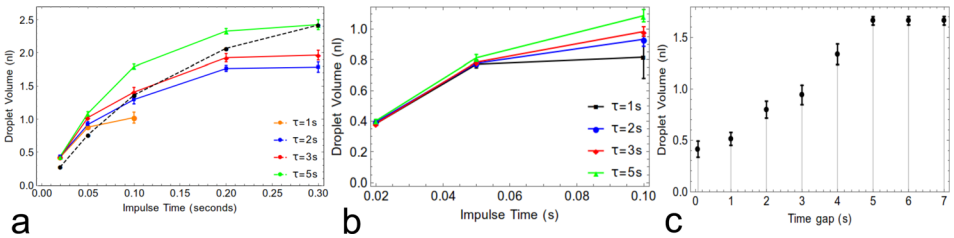

FIG. 6. Effect of impulse time and time gap between two successive impulses on size of droplet. Different gaps (τ=1 – 5 s) between two successive impulses at fixed flow rates are shown at 20 μl/h in the main channel and (a) 80 μl/h (b) 40 μl/h in the nozzle flow-by input channel. For each impulse time, statistical data on droplet volumes are collected up to 30 min. In the plot (a), the dashed black line shows the theoretical prediction of the equivalent circuit model (see Sec. III E), corresponding to long gap times (green 5 s curve). (c) Flow rates in side channel: 80 μl/h, central channel: 20 μl/h, impulse time: 0.1 s. After 4 s, the average size of droplet size stays constant (which is due to complete relaxation of interface).

compliance (elasticity) effects of the PDMS channels, connecting tubes and syringes (see Sec. III E) and due to the presence of multiple phases with different surface properties.

The above considerations limit the programmable rate of droplet formation in the microfluidic device. So the performance of the DoD microfluidic device depends on three parameters: impulse time, time gap between successive impulses, and flow rates. For defined flow rates and impulse time, there is a finite relaxation time for the two-phase interface to become stably positioned again. If the gap between successive impulses is less than the relaxation time, the droplet size becomes smaller and less consistent as shown in Figures 6(b) and 6(c). It also depends on the flow rate of the side channel. The higher the flow rate in a side channel, the faster the interface moves back to a stable position. This is due to creation of a stronger restoring force on the interface, just after the end of impulse. The larger the flow in the side-channels must be, the larger will be the consumption of chemical samples. Fig. 6(c) reveals the approx. relaxation time of the interface. It confirms that the size of droplet becomes independent of the gap once complete relaxation occurs at the interface.

D. Two phase flow simulation of droplet generation at a nozzle

Using the theoretical CFD framework (as described in Sec. II G), we studied the behavior of the injection nozzles in 2D and 3D simulations. We investigated droplet formation by simulating a pressure impulse in the side channels against the flow (dispersed aqueous phase, density

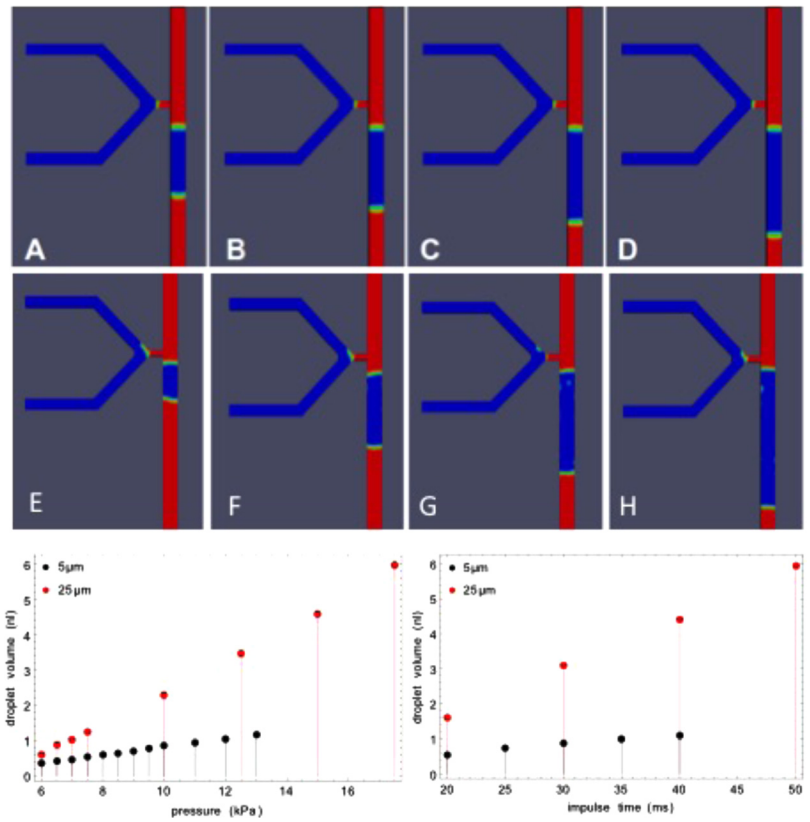

FIG. 7. Droplet volume dependence on impulse time and applied pressure for two nozzle heights. The images show one characteristic time point in the simulation for different impulse times: top row 5 μm, middle row 25 μm nozzle heights. Impulse times for images (A)–(D) are 20, 25, 30, and 40 ms and (E)–(H) are 20, 30, 40, and 50 ms, while keeping the applied pressure fixed to 9 and 7.5 kPa, respectively. The simulation was performed using open source software (see Sec. II G), with appropriate lateral channel dimensions for the real devices: 100 μm (Length) by 40 μm (width). Stable simulations could be performed with increasing numbers of finite elements and run times down to 5 μm nozzle height. Plots left: droplet volume as function of injection impulse time. Right: droplet volume as function of applied pressure with fixed injection impulse time (20 ms).

1000 kg/m^3, and kinematic viscosity 1×10^{-6} m^2/s). This leads to pressure build up at the nozzle and the formation of a droplet (inside the continuum phase, density mineral oil 845 kg/m^3, and kinematic viscosity 1.5×10^{-5} m^2/s). An example of the top view of the 3D simulations is shown in Fig. 7, varying the length of time for which the pressure pulse (originating from the pinch valve) is applied, or the pressure value itself (supplementary material[35] Fig. S11). The plotted injected volumes shown in Fig. 7 demonstrate the linearity of the dosage response to injection time, for constant input pressure. Similar droplet generation phenomena were observed at both 25 μm and 5 μm (images in Fig. 7). Extrapolation must be performed down to the 1–2 μm nozzle height in the real device since direct simulation is hindered by the phase interface modeling resolution and computational resources. The pressure dependence exhibits a threshold phenomenon because of the finite interfacial pressure.

According to these simulations, droplet size can be adjusted as required, by changing the impulse time and applied pressure: both exhibit linear domains. The time varying pressure from the pinch valve (see Sec. III E) is responsible for nonlinear saturation effects in the impulse time dependence in real experiments (see Fig. 6), but we employed impulse time in the main injection experiments to control volume in the range of a few nl. The ratio of flow rates in the main channel to the side channel was found to be important for the stability of the interface at the nozzle tip. We observed that by increasing the flow rate ratio (continuum phase to dispersed phase), the interface becomes unstable, and leads to inconsistent droplet formation. A viable window of parameters for robust droplet control was determined experimentally. To complete the tie-up between theory and experiment, we need to embed the model in a larger system including the external control devices: We do this using hydrodynamic equivalent circuit modeling.

E. Hydrodynamic equivalent circuit simulation of droplet on demand generation

The local two-phase flow simulations show that appropriate pressure pulses can indeed generate droplets over a hydrodynamic barrier nozzle of the type and dimensions exhibited in the real device. However, in the real microfluidic device, the pressure pulse is generated remotely through a pinch valve in combination with a tuneable hydrodynamic resistor downstream and the elasticity of connecting capillaries and PDMS structures must affect the performance of droplet generation and injection. Moreover, we need to check that the values employed for pressure pulses in the two-phase simulations correspond to those involved in the real device, and that droplet generation is robust to the operation of other nozzles. In order to check these criteria, we developed an equivalent circuit to describe the combination of the external syringe, pinch valve, and tuneable resistor external devices, with connecting tubing and the microfluidic device, also including up to two nozzles in the circuit to explore mutual interference effects (Sec. II G).

The equivalent circuits, including the elastic properties of the channels and capillaries, are shown in Figure 8, for a dual nozzle subsystem. The single nozzle system was also simulated and is seen as a subset indicated by the dashed rectangle. The calculated values for the hydrodynamic resistors and capacitors are summarized in the supplementary material[35] Table S12. The syringe pumps are constant current inputs, and the fluid is switched solely by the electronic pinch valve. The timing parameters for the pinch valves involved 5 ms switching with two time parameters t_{on} and t_{gap} with default values of 0.1 s and 0.2 s. The pinch valve can be modeled in detail as an elliptical compression of the circular tube (see supplementary material[35] Fig. S13 and description there), but the result is a nearly linear volume injection into the sample exit tube (ca. 300 nl) and a sharp increase in resistance near the end of the closing stroke (because of the inverse cubic dependence on channel height near closing), so that this can be sufficiently modeled as a step function (taking compliance effects into account). During the closing process, a substantial part of the valve volume exits over the tuneable resistor, while only a nl scale volume is injected.

We then used the hydrodynamic equivalent circuit simulations to investigate three aspects of the droplet injection design for a single nozzle: (i) the tuneable resistor values in the full

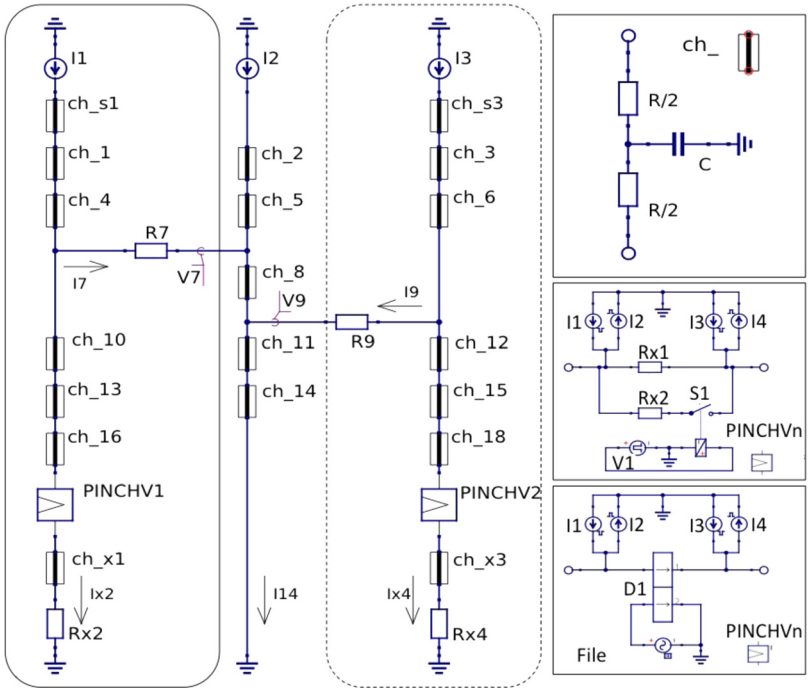

FIG. 8. Equivalent hydrodynamic circuits for embedding of microfluidic nozzles with control system. The circuit diagram contains two subcircuit elements ch_n and PINCHVn which are depicted in boxes on the right. The flow-by input and nozzle 1 is on left, the carrier channel into which the droplet is injected in the middle, and nozzle two optionally within the dashed border on the right. Further nozzles can be included modularly like nozzles 1 and 2. Simulations were performed with one nozzle to characterize performance and two nozzles to check interference. If the circuit elements marked ch_n are simply resistors, the circuit is a purely resistive circuit with instantaneous response. Top right: circuit with equivalent capacitors for the elasticity of the PDMS channels, capillaries and syringes. Bottom right: two different circuit implementation of the pinch valves: upper with a simple switch (open when pinch valve shut, and vice versa) operated at the end of the closing stroke to increase the internal resistance to the high pinched value; lower with a stroke dependent resistance and flow profile (see also supplementary material[35] S13) derived from elliptical pinch compression of the silicone tube.

range relevant to control, (ii) the nozzle resistance over values determined from experimental nozzle heights in the range 1–2 μm, and (iii) the width of the outflow channel on the sample side of the nozzle. The parameter variations of nozzle pressure and flow rate for these three cases are shown in Fig. 9. The results confirm that (i) the tuneable resistors in the 10^{15} Pa s/m^3 range ($\approx$1 GΩ) are required to transfer enough pressure to allow nanoliter scale injection; (ii) nozzle resistors also affect the delivery volume and response time of the device, which is longer than the 5 ms switching time of the pinch valve because of compliance effects, mainly of the pinch valve itself; and (iii) a larger sample exit channel width is necessary, to ensure that the volume flow from the pinch valve reaches the nozzle. We also predicted the injection flow rate Fig. 9(g) and volume as a function of pinch valve closed time (impulse time). The predicted volumes are compared with experiment in Fig. 6(a), reproducing the nonlinear saturation behavior of injection volume semi-quantitatively. Residual differences are attributable to uncertainties in the actual values of tuneable resistors and pinch valve compliances. The two nozzle system was then simulated to explore potential interference effects between nozzles in Figs. 9(h) and 9(i). The scale blowup makes the influences visible, but they are not sufficient to overcome the restoring forces associated with the two-phase fluid interface, and thus allow independent operation.

F. Injection into mixed droplets and statistics

The injection mixing process is demonstrated in the supplementary material[35] Movies S4–S6, using volume monitoring and absorption dyes for coloring. We also could follow the generation and mixing process for droplets from aqueous samples of DNA using fluorescent

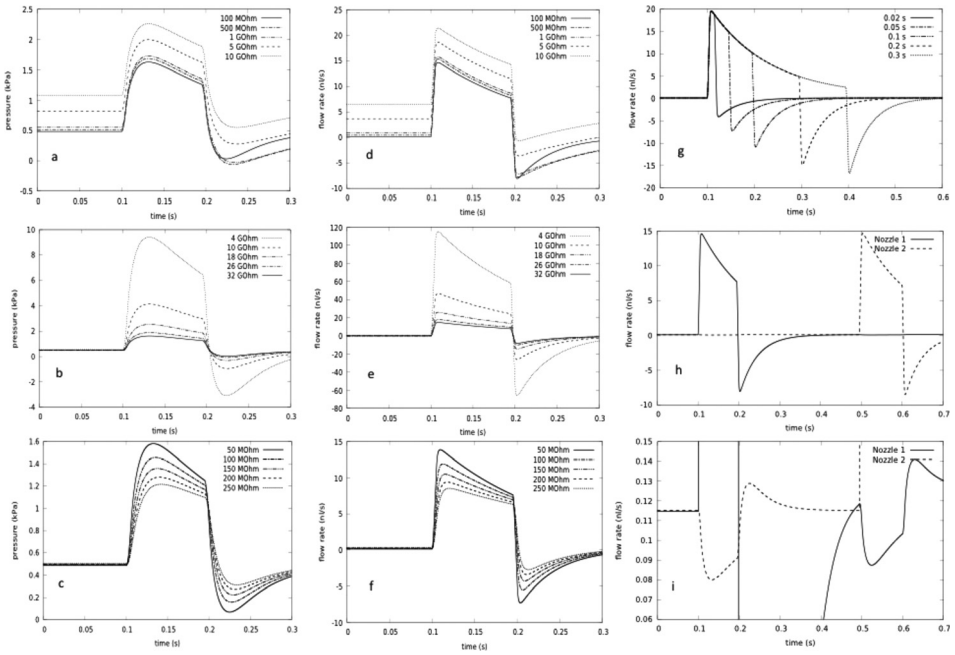

FIG. 9. Equivalent circuit calculation of droplet generator nozzle pressure and flows: The pressures are all relative to atmospheric pressure at the nozzle inputs, and the flow rates are those over the nozzles. All values of components apart from those explicitly varied are taken from the supplementary material Table S11.[35] (a)–(g) One nozzle circuit from Fig. 10. (h) and (i) Two nozzle circuit. Hydrodynamic resistance parameter values are displayed as electrical equivalent with 1 $G\Omega = 10^3$ $M\Omega \approx 10^{15}$ Pa s/m^3 = 1 kPa s/nl $\cong$ 10 mbar s/nl. (a) and (d) Pressure and flow rate profile during injection as a function of tuning resistor. (b) and (e) Pressure and flow rate profile during injection as a function of nozzle resistance (corresponding to nozzle ledge heights 1–2 μm). (c) and (f) Pressure and flow rate profile during injection as a function of microfluidic channel resistance at sample exit (varying from narrower input channel to broader realized exit channel resistance). (g) Droplet flow rate as a function of impulse time. (h) and (i) Independent operation of two nozzles. The influence of one nozzle on the other is only visible in the blowup scale of e′. Flow rates: central channel: 20 μl/h, side channel: 100 μl/h, impulse time is 0.1 s, unless otherwise specified.

labeling with Alexa dyes, see Figure 10, and especially that the creation process also allows for mixed droplets. Downstream surfactant addition is important in enabling low-surfactant content during and facilitating injection. In the series of pictures shown, mixing of droplets is already nearly finished after a few seconds, due to the small dimensions allowing for rapid diffusion and the inner convective dynamics (although droplet mixing is quite complex, driven by Poiseuille-flow,[41] wall lubrication, and Marangoni effects).

The statistics of injection mixing volumes under programmable control are evaluated experimentally in Fig. 11, with a comparison between predicted and experimental mixed volumes proving excellent agreement for binary and ternary mixing.

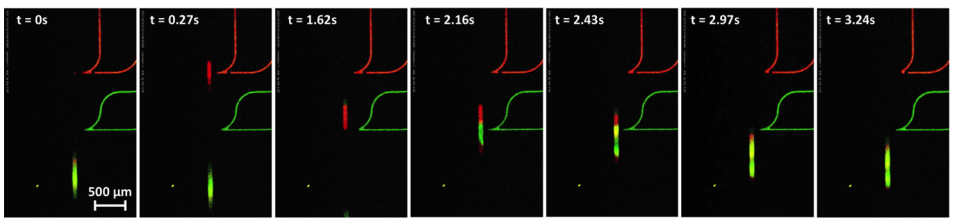

FIG. 10. Mixing of DNA-droplets: on-chip verification with fluorescence labeling. Two different DNA-solutions with short end-labeled oligos are used to create arbitrary droplet combinations. In this case, the second DNA solution (green fluorescent) is injected into the droplet with the red fluorescent dye. The mixing of both solutions inside the combined droplet is almost finished after a few seconds. The dynamics is also documented in supplementary material[35] Movie S7.

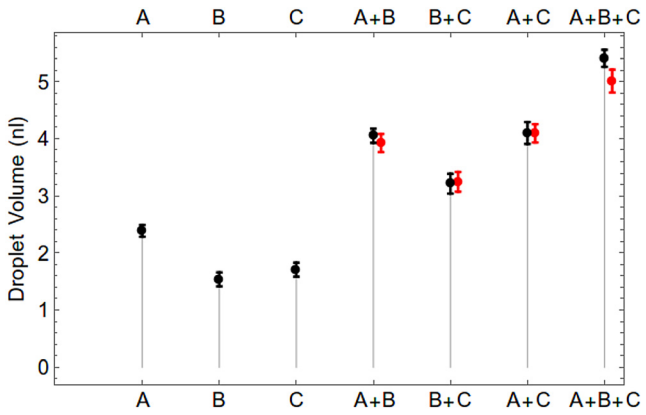

FIG. 11. Statistics of mixing up to three injection channels (A, B, C), Droplets were created using three input nozzles to create different mixing combinations by programming the timings for successive injections, A, B, C (black) shows statistics with single input. For A + B, B + C, C + A, A + B + C, black points shows observed statistics of mixing and red points shows expected value calculated from single injections.

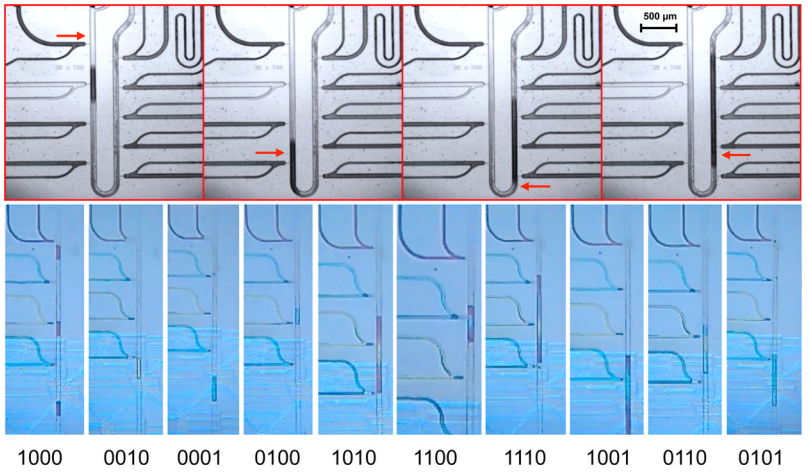

FIG. 12. Programmable droplet generation, injection, and mixing. Top: mixing droplets from 4 out of 9 nozzles: the red arrows mark the point of injection in the time series. Bottom: Creation of droplet packets, including mixing at some of the droplets. The bits shown at the bottom of the single images denote which nozzle is active in the shown slice. For example, in the first slice, only red colored droplets are created, in the second red and yellow, and in the third only the last blue nozzle is active.

G. Programmed sequences of droplets

The final test of a droplet-on-demand system is the creation of programmed droplet sequences with defined contents (see Figure 12). For subsequent export of droplets, the combinatorial production of programmable chains of droplets with different DNA proved more robust than mixed droplets and was adopted as the primary mechanism, when the device was scaled up to 8 inputs. On chip mixing has the additional advantage of supporting on-chip reactions, but this is not essential for many applications, such as the creation of DNA libraries,[9] because of parallel MWP-based assembly PCR (polymerase chain reaction) capabilities.

IV. CONCLUSION

The major parameter defining the quality of droplets created is the surface tension of the two fluids interacting with each other. However, the thickness of lubricating layers of carrier fluid and the influence on droplet stability is complex at these scales despite the low Reynolds number flow. Extensive studies of droplet coalescence and transport properties in channels have

been made, see Refs. 11, 42, and 43 and references therein. Our approach has been to perform nanoscale pipetting with no or only small quantities of surfactant (insufficient for long term droplet stabilization) as this not only improves pipetting performance stability but also allows injection delivery into passing droplets. The droplets are then stabilized downstream with an additional carrier fluid input from either side, ready for export. We have concentrated on the performance of aqueous droplet systems, as this is our main application area, but have included cases of significant enzyme content, which affects the surfactant properties of the droplets. The volume performance statistics of our device are competitive at 2.5% with traditional pipetting volume fluctuations for single nozzles (at the $\leq$5% level) but careful tuning of the device after filling is necessary to ensure balanced operation when multiple nozzles are used. Further work is needed to fully explore the plateau of stability of the droplet generation within this device. We have characterized and optimized our device by modeling both with two-phase flow CFD and with equivalent hydrodynamic circuits including compliance, comparing theory, and experiment. Another advantage of our approach is that the combinatorial inputs are flow-by inputs right up to the nozzles, allowing self-cleaning of samples without any fluidic contacts prior to droplet formation.

Although the number of on chip parallel inputs may be extended from the level of 8 or 9 in this work, e.g., to 16 by straightforward extension of the current work, and this is already sufficient for many potential experiments and applications, the full benefit of programmable combinatorial pipetting at the nanoscale can only be reached if a significantly larger number of inputs is achieved. The current device, with its modular separation of flow-by pressure inputs from the droplet carrier channel, is well suited to making use of combinatorial chains of input plugs to enhance the total number of inputs that can be processed without re-plumbing connections, cf. Refs. 11 and 17. Then such devices can be connected to MWPs via serial pipetting robots or electronic pipettes.

The performance of the droplet generator in terms of timing of droplets is only in the fractional Hz range, whereas with integrated piezoelectric driving of pressure impulses, DoD delivery can be achieved at the rate of 50 or 100 Hz (Ref. 44) and kHz rates have been achieved with electrical interface control devices such as the picoinjector.[27] However, the ease of integration of the current system with other custom microfluidics sets it apart, since only single layer PDMS microfluidics is required and combinations with other functionalities are straightforward (see also supplementary material[35] Fig. S8), and a combination of techniques in future may result in a system with both high frequency and the facile modularity of the current approach. The impact of this work will not only be to allow more sophisticated tests of droplet hydrodynamic theory (as discussed in Ref. 11) but also to combinatorial tasks in low volume reaction chemistry as, for example, in the creation of DNA libraries.[11]

The device does not make use of the electronic on-chip processing of chemical microprocessors originally investigated by the authors for iterative rounds of synthesis and product cleanup, but could be combined with on chip microfluidic reaction processing to allow iterative algorithms to be employed. It also allows a ready integration with electronic microfluidics as in Ref. 33, as shown in Fig. 6(d) and in an earlier version in supplementary material Fig. S8,[35] and so could form the basis for integrated droplet processing involving separation.[34]

In summary, we have presented a novel single layer microfluidic device that allows versatile droplet-on-demand mixing and sequencing of nanoliter droplets from many inputs at rates up to a few Hz. While commercial devices are now available for droplet sequencing (e.g., Dolomite), the current principle allows straightforward integration with other microfluidic operations in the single layer PDMS without additional on chip control interfaces, it is accessible to numerous research labs and could provide a valuable enabling technology for the more widespread shift to nanoliter scale experimentation.

ACKNOWLEDGMENTS

This research leading to these results has received funding from the European Union Seventh Framework Program (FP7/2007-2013) under Grant Agreement No. 265505 (CADMAD) and, in

part for some early precursors of the droplet generator chip, under Grant Agreement No. 249032 (MATCHIT). The authors wish to thank Jana Bagheri and Thomas Maeke for their assistance with biochemical tests, gel-preparation and analysis, implementation, and set-up.

[1]T. V. Murthy, D. Kroncke, and P. D. Bonin, J. Lab. Autom. **16**(3), 221 (2011).
[2]W. Gaisford, J. Lab. Autom. **17**(5), 327 (2012).
[3]A. C. Hatch, J. S. Fisher, A. R. Tovar, A. T. Hsieh, R. Lin, S. L. Pentoney, D. L. Yang, and A. P. Lee, Lab Chip **11**(22), 3838 (2011); A. B. Theberge, E. Mayot, A. E. Harrak, F. Kleinschmidt, W. T. S. Huck, and A. D. Griffiths, *ibid.* **12**(7), 1320 (2012).
[4]L. Mazutis, A. F. Araghi, O. J. Miller, J. C. Baret, L. Frenz, A. Janoshazi, V. Taly, B. J. Miller, J. B. Hutchison, and D. Link, Anal. Chem. **81**(12), 4813 (2009).
[5]A. Schober, R. Günther, A. Schwienhorst, and M. Döring, Biotechniques **15**(2), 324–329 (1993).
[6]M. G. Simon and A. P. Lee, in *Microdroplet Technology: Principles and Emerging Applications in Biology and Chemistry, Integrated Analytical Systems*, edited by P. Day *et al.* (Springer Science + Business Media, LLC, 2012), Chap. 2, pp. 23–50; M. Joanicot and A. Ajdari, Science **309**(5736), 887 (2005); R. Seemann, M. Brinkmann, T. Pfohl, and S. Herminghaus, Rep. Prog. Phys. **75**(1), 016601 (2012); M. T. Guo, A. Rotem, J. A. Heyman, and D. A. Weitz, Lab Chip **12**(12), 2146 (2012); T. M. Tran, F. Lan, C. S. Thompson, and A. R. Abate, J. Phys. D: Appl. Phys. **46**(11), 114004 (2013); S.-Y. Teh, R. Lin, L.-H. Hung, and A. P. Lee, Lab Chip **8**(2), 198 (2008).
[7]R. Blanc, G. Castellan, C. Chabrol, N. David, E. Dubard, O. Constantin, Y. Fouillet, D. Jary, A. Rival, P. Caillat, and C. Delattre, in *μTAS 2008* (San Diego, 2008), p. 1696; M. G. Pollack, R. B. Fair, and A. D. Shenderov, Appl. Phys. Lett. **77**, 1725 (2000).
[8]S. K. Cho, H. Moon, and C.-J. Kim, J. Microelectromech. Syst. **12**(1), 70 (2003).
[9]U. Tangen, P. F. Wagler, S. Chemnitz, G. Goranovic, T. Maeke, and J. McCaskill, ComPlexUs **3**(1–3), 48 (2006).
[10]U. Tangen, G. K. A. Minero, A. Sharma, P. F. Wagler, R. Cohen, O. Raz, T. Marx, T. B. Yehezkel, and J. S. McCaskill, "DNA-library assembly programmed by on-demand nanoliter droplets from a custom microfluidic chip," ACS Synth. Biol. (submitted).
[11]A. Sharma, U. Tangen, and J. S. McCaskill, "Lead-controlled transport of combinatorial microdroplet trains exported from microfluidic chips," Microfluid. Nanofluid. (submitted).
[12]J. Melin and S. R. Quake, Annu. Rev. Biophys. Biomol. Struct. **36**(1), 213 (2007); J. Wang, H. C. Fan, B. Behr, and S. R. Quake, Cell **150**(2), 402 (2012).
[13]W. Wang, C. Yang, and C. M. Li, Small **5**(10), 1149–1152 (2009); H. Song, D. L. Chen, and R. F. Ismagilov, Angew. Chem., Int. Ed. **45**(44), 7336 (2006).
[14]J.-C. Baret, Lab Chip **12**(3), 422 (2012); C. Holtze, A. C. Rowat, J. J. Agresti, J. B. Hutchison, F. E. Angilè, C. H. J. Schmitz, S. Koster, H. Duan, K. J. Humphry, R. A. Scanga, J. S. Johnson, D. Pisignano, and D. A. Weitz, *ibid.* **8**(10), 1632 (2008).
[15]See http://www.tecan.com/platform/apps/product/index.asp/?MenuID=3812&ID=8113&Menu=1&Item=21.1.12 for Hewlett Packard/Tecan Picoliter digital dispensing technology.
[16]P. F. Wagler, J. S. McCaskill, and T. Foster, Patent No. EP1521631 (13 April 2005).
[17]F. Gielen, L. van Vliet, B. T. Koprowski, S. R. A. Devenish, M. Fischlechner, J. B. Edel, X. Niu, A. J. Demello, and F. Hollfelder, Anal. Chem. **85**(9), 4761 (2013).
[18]J. Guzowski, P. M. Korczyk, S. Jakiela, and P. Garstecki, Lab Chip **11**(21), 3593 (2011).
[19]K. Churski, J. Michalski, and P. Garstecki, Lab Chip **10**(4), 512 (2010).
[20]S. Zeng, B. Li, X. Su, J. Qin, and B. Lin, Lab Chip **9**(10), 1340 (2009).
[21]F. Guo, K. Liu, X.-H. Ji, H.-J. Ding, M. Zhang, Q. Zeng, W. Liu, S.-S. Guo, and X.-Z. Zhao, Appl. Phys. Lett. **97**(23), 233701 (2010).
[22]R. Lin, J. S. Fisher, M. G. Simon, and A. P. Lee, Biomicrofluidics **6**(2), 024103 (2012).
[23]A. K. Au, H. Lai, B. R. Utela, and A. Folch, Micromachines **2**, 179 (2011).
[24]Y. Zeng, M. Shin, and T. Wang, Lab Chip **13**(2), 267 (2013).
[25]J. Tang, A. M. Jofre, R. B. Kishore, and J. E. Reiner, Anal. Chem. **81**(19), 8041 (2009).
[26]J. Xu and D. Attinger, J. Micromech. Microeng. **18**(6), 065020 (2008).
[27]A. R. Abate, T. Hung, P. Mary, J. J. Agresti, and D. A. Weitz, Proc. Natl. Acad. Sci. **107**(45), 19163 (2010).
[28]S.-Y. Park, T.-H. Wu, Y. Chen, M. A. Teitell, and P. Y. Chiou, Lab Chip **11**(6), 1010 (2011).
[29]X. Niu, M. Zhang, J. Wu, W. Wen, and P. Sheng, Eur. Phys. J. E-Soft Matter **5**, 576 (2009).
[30]T. Andrukh, B. Rubin, and K. G. Kornev, Langmuir **27**, 3206–3210 (2011).
[31]S. Mishra, K. L. Barton, A. G. Alleyne, P. M. Ferreira, and J. A. Rogers, J. Micromech. Microeng. **20**(9), 095026 (2010).
[32]H. Zec, T. D. Rane, and T.-H. Wang, Lab Chip **12**(17), 3055–3062 (2012).
[33]P. F. Wagler, U. Tangen, T. Maeke, and J. S. McCaskill, Biosystems **109**(1), 2 (2012).
[34]P. F. Wagler, U. Tangen, J. Ott, and J. S. McCaskill, "General-purpose, parallel and reversible microfluidic interconnects," IEEE Trans. Compon., Packag., Manuf. Technol. (in press).
[35]See supplementary material at http://dx.doi.org/10.1063/1.4907895 for 13 supplementary movies, table, and figures illustrating dynamics and additional aspects of device performance.
[36]See http://www.openfoam.org/docs/user/ for OpenFOAM (Version 1.5 user's guide).
[37]C. W. Hirt and B. D. Nichols, J. Comput. Phys. **39**(1), 201 (1981).
[38]See http://www.salome-platform.org/ for Salome Platform.
[39]K. W. Oh, K. Lee, B. Ahn, and E. P. Furlani, Lab Chip **12**(3), 515 (2012).
[40]D. Van Noort and J. S. McCaskill, Nat. Comput. **3**(4), 395 (2004).
[41]H. Kinoshita, S. Kaneda, T. Fujii, and M. Oshima, Lab Chip **7**(3), 338 (2007).
[42]C. N. Baroud, F. Gallaire, and R. Dangla, Lab Chip **10**(16), 2032 (2010).
[43]J. Maddala, S. A. Vanapalli, and R. Rengaswamy, Phys. Rev. E **89**, 023015 (2014).
[44]S. Jakiela, P. Debski, B. Dabrowski, and P. Garstecki, Micromachines **5**(4), 1002 (2014).
[45]Dr. Porada, Uni Stuttgart, Germany, personal communication, 2013.